Title

Evaluation of remote sensing-based evapotranspiration models against surface renewal in almonds, tomatoes and maize

Authors

Xue, Jingyuan
Bali, Khaled M
Light, Sarah
et al.

Publication Date

2020-08-01

DOI

10.1016/j.agwat.2020.106228

Peer reviewed

Evaluation of remote sensing based evapotranspiration models against surface renewal in almonds, tomatoes and maize

Jingyuan Xue[1, 2], Khaled M. Bali[3], Sarah Light[3], Tim Hessels[4], Isaya Kisekka[1*]

*Corresponding author: Isaya Kisekka

[1]Department of Land Air & Water Resources, and Department of Biological and Agricultural Engineering University of California Davis, Davis, CA, 95616, USA

[2]College of Water Resource and Civil Engineering, China Agricultural University, Beijing 100083, China

[3]Kearney Agricultural Research and Extension Center, University of California, Parlier, CA 93648, USA

[4] Department of Water Management, Delft University of Technology, Stevinweg 1, 2628 CN Delft, Netherlands

* Corresponding author: Isaya Kisekka, Department of Land Air & Water Resources, and Department of Biological and Agricultural Engineering University of California Davis, Davis, One Shields Avenue, CA 95616-5270, USA, E-mail: ikisekka@ucdavis.edu

Abstract:

Evapotranspiration (ET) is a major hydrologic flux used in water resources planning and irrigation management. While recent advances in remote sensing (RS) have enabled availability of high spatial and temporal resolution ET data, a lack of information related to error in the estimations has made it challenging to use this data for on-farm irrigation management decision making. In this study, three commonly used single-source RS ET models (pySEBAL- a new version of Surface Energy Balance Algorithm for Land; SEBS-Surface Energy Balance System algorithm; and METRIC - Mapping Evapotranspiration at High Resolution with Internalized Calibration) were used to estimate daily actual evapotranspiration (ET_a) for almond, processing tomato, and maize in the Central Valley of California. Model evaluation was conducted by comparing the predicted ET_a from RS with in-situ measured ET_a using surface renewal. Results indicated that the RS-based ET_a estimations for all three models were within acceptable levels of uncertainty and agreed well with surface renewal estimates except for the underestimation by pySEBAL and METRIC during early season growth stages of processing tomatoes. This underestimation was attributed to the lack of accuracy when using single source ET models under lower vegetation cover condition (when ET is dominated by soil evaporation). Better estimates of ET_a with pySEBAL and METRIC were detected at full cover, which explains the applicability of these two models to irrigation management during peak crop water demand. SEBS performed the best among the three RS-based models for daily ET_a estimation for all crops. This suggests that SEBS-based ET_a estimates can be adopted in operational irrigation management programs for farms that have not installed in field ET sensors such as Tule Sensors (Tule Technologies Inc.). In addition, RS based ET is spatially distributed which can help to identity spatial variability between different irrigation zones.

Keywords: Remote sensing; daily evapotranspiration; pySEBAL; METRIC; SEBS; Surface renewal.

1. Introduction

Climate change and population growth have put a lot of pressure on the finite fresh water resources on the earth (Mancosu et al., 2015; Nyolei et al., 2019). California's Central Valley is one of the most productive agricultural regions in the world. According to the recent USDA Irrigation and Water Management Survey, in 2018 California had approximately 3.403 million hectares of irrigated farmland (USDA, 2018). California's agriculture is very diverse ranging from livestock, to field crops and specialty crops. According to the California Department of Food and Agriculture, in 2018 California farms and ranches received approximately $50 billion dollars in cash receipts for their output (CDFA, 2018). However, the recent multi year drought, competition for water from other users (urban and environmental), and groundwater depletion threaten sustainability of California's irrigated agriculture. To remain viable, California farmers will need to optimize agricultural water management by increasing water productivity through adoption of advanced management practices such as site-specific zone irrigation Management.

Recent new water regulations such as the Sustainable Groundwater Management Act (SGMA) will be forcing farmers to adapt to constrained water supplies when the new regulations are fully implemented. ET is a major hydrological flux that links water, energy, and carbon cycles, and plays an important role in hydrology, meteorology, and agricultural water management (Li et al., 2009; Su, 2002; Anderson et al., 2008; Allen et al., 2011a; Hu et al., 2018; Zhao et al., 2013). Site-specific irrigation management requires knowing crop ET_a for each management zone. Conventional ET estimation techniques, such as Bowen ratio, eddy covariance, surface renewal, weighing lysimeter, soil water balance, and scintillometer, can provide relatively accurate estimates of ET_a at field scale but are not spatially explicit and some are expensive and not readily available to growers (Wang and Dickinson, 2012; Long et al., 2014). The ability of remote sensing based models to provide ET_a at high spatiotemporal resolutions makes them suitable for scaling up and commercialization in precision agricultural water management (Lian and Huang, 2016; Rango, 1994). Because of its potential benefits, this topic has attracted a lot of attention from researchers over the past several decades (Bastiaanssen et al., 1998; Su, 2002; Jiang and Islam, 1999; Allen et al., 2007a; Senay et al., 2016). Despite differences in theory and complexity of these models, they generate reasonable ET_a maps for different specific conditions with acceptable error and uncertainty (Khan et al., 2010; Tasumi and Kimura, 2013).

Most RS-based ET_a estimation models estimate only instantaneous or daily ET_a on the satellite overpass date, while most practical applications in water resources and agricultural managements long require time-series of daily ET_a at the field scale. Therefore, it is essential to obtain long time-series estimates of ET_a. Landsat 8 provides an opportunity for an 8-day overpass frequency (usable images can be impacted by clouds) which makes it suitable for monitoring water use and vegetation conditions. Landsat allows calculation of the Normalized Difference Vegetation Index (NDVI) at 30 m resolution. Land surface temperature is acquired at different spatial resolutions based on the Landsat mission (120 m for the thermal band in Landsat 5, 60 m for Landsat 7, and 100 m for Landsat 8). Landsat also provides the longest most continuous measurements of relevant bands for agricultural water management. Over the past two decades, RS-based ET models using Landsat imagery have been validated both at the field scale and the regional scale (Mohamed et al., 2004; Whitfield et al., 2011; Bastiaanssen et al., 2002; Allen et al., 2007a; Evett et al., 2012).

The most commonly used RS based ET_a models can be divided into two categories. The first is based on semi-empirical methods using vegetation indices from surface reflectance data to estimate crop coefficients (K_c) and then calculating ET_a using the estimated K_c and reference evapotranspiration (ET_0), and the second on biophysical processes such as the surface energy balance. One major weakness of the semi-empirical models is the requirement of prior knowing site-specific parameters, which limits the application of these models to estimate ET_a over regional scales with variable surface conditions. ET_a estimation models based on the surface energy balance can be divided into two groups: one-source and two-source models. One-source models consider soil and vegetation as an integration with a unified surface temperature to do land surface energy exchange (Bastiaanssen et al., 1998; Allen et al., 2007b; Su, 2002; Carlson, 2007; Senay et al., 2007). Two-source models simulate evaporation and transpiration separately (Norman et al., 1995; Zhang et al., 2005; Mu et al., 2011; Long and Singh, 2012). The most difficult part in using two-source ET models are that they require the pre-knowledge of surface temperature of soil and vegetation, which is usually not directly obtainable from satellite images. Thus, single-source models are often used among many RS-based ET estimation models: e.g., Surface Energy Balance Algorithm for Land (SEBAL) (Bastiaanssen et al., 1998), Mapping Evapotranspiration at High Resolution with Internalized Calibration (METRIC) (Allen et al., 2007b), the Simplified Surface Energy Balance (SSEB) (Senay et al., 2007) and the Surface Energy Balance System (SEBS) (Su, 2002). SEBAL has long been recognized as the most suitable RS-based model to estimate ET_a without prior knowledge of the field conditions, such as crop types, soils and management practices (Bastiaanssen et al., 2005; Nyolei et al., 2019). The SEBAL model and its variant METRIC model employ the contextual method in ET estimation, in which pixel-wise sensible heat flux and latent heat flux are calculated under the constraint of selected hot and cold extreme pixels within an area of interest. It uses the information of the whole satellite image for the estimation of ET_a at each pixel. SEBS, based on single-pixel method, calculates sensible heat flux (H) and latent heat flux (λE) by solving the surface energy budget for each pixel independently from other pixels, which requires the ground observation of vegetation height, surface wind speed and air temperature.

SEBAL and METRIC, employ the contextual method that requires the user to select "anchor" pixels with extreme temperature and vegetation conditions, which affects the accuracy of these models for ET_a estimation when/where a hot/cold pixel cannot be easily selected by the user. Consequently, selecting pixels manually causes bias in ET_a estimation, and the process of manually selecting anchor pixels is time-consuming and subjective. To overcome the challenges of manual anchor pixel selection, semi-automated and automated selection procedures to identify cold and hot pixels were developed recently (Jaafar and Ahmad, 2019). This work demonstrated that semi-automated and automated anchor pixel selection procedures could be used to identify hot and cold pixels based on parameters characterizing extreme conditions in the satellite image, such as surface albedo, roughness length, land surface temperature, and NDVI. A new python version of SEBAL model 3.0, pySEBAL, incorporates an automation pixel selection procedure and is currently under development and testing at the IHE-Delft Institute (UNESCO-IHE, 2018). Bhattarai et al. (2017) proposed a fully automated procedure and applied it to SEBAL and METRIC models based on an exhaustive search algorithm, and the comparison of the ET_a results with manual pixel selection procedures showed good agreement. Although the automated pixel selection procedure still requires pre-defined information of the hot and cold pixels, this technique can help in eliminating user subjectivity.

Spatial field-scale ET_a estimation from RS-based models are widely used in irrigation management. They provide the amount of water that needs to be applied to each irrigation zone to meet crop water needs (Sanchez et al., 2017). Validation of ET_a results from RS-based models are usually done using conventional ground-based ET_a measurement techniques such as weighing lysimeters and micrometeorological methods (eddy covariance, surface renewal, Bowen ratio energy balance, etc.). Allen et al. 2011b concluded that considerable accuracy of ground-based ET_a measurements can be obtained once these instruments were correctly installed and operated. Most of these ground-based ET_a measurement techniques are expensive to implement and need to be installed and operated by experienced technicians (Snyder et al., 2008).

However, simpler micrometeorological approaches such as surface renewal can significantly reduce cost but require trained technicians to operate properly. With the surface renewal, crop ET_a can be determined by calculating it as the residual of the energy balance. H derived from the surface renewal techniques obtained by a simpler and less expensive method, which uses fine wire thermocouples to measure high frequency air temperatures at the surface-atmosphere interface (Mengistu and Savage, 2010; Hu et al., 2018; Shapland et al., 2012). In general, surface renewal measurements costs much less than many other ground-based ET measurement techniques such as eddy covariance, thus it provides a low-cost way to measure crop ET_a but requires measuring or estimating net radiation. As early as 1995, Kyaw et al. (1995) reported that the surface renewal method could be used accurately for stable conditions for canopies of 6 m high or lower, and calibration against eddy covariance or other methods may be needed under unstable conditions when the surface renewal errors are greater. Later, the application of surface renewal in ET_a estimation has been conducted for various crops, including processing tomato (Rosa et al., 2013), grapevine (Spano et al., 2000), pecans (Simmons et al., 2007), cotton (Payero and Harris 2010), etc. Good correction between surface renewal method and other ground-based ET measurements, such as lysimeters and eddy covariance, were reported in these researches. These results, however, are preliminary and additional testing with other crops and environments are now underway. Great potential has been demonstrated for using the surface renewal method as a cheaper alternative to lysimeters and eddy covariance for directly measuring daily ET. In California, the surface renewal approach has been successfully commercialized by Tule Technologies Inc. (http://www.tuletechnologies.com/). The farmer pays an annual subscription fee, the company processes surface energy fluxes, and delivers field specific daily ET_a to the farmer. Since 2017, many studies reported the good correlation between the ET estimations from the Tule Technologies surface renewal stations and eddy covariance flux towers (Fulton et al., 2017; Rieger, 2017; Zaccaria et al., 2017; Montazar et al., 2018).

There is a need to compare this new technology with existing remote sensing models. The objectives of this study were to 1) compare ET_a from three remote sensing based models (pySEBAL, METRIC, and SEBS) to ground-based measurements from surface renewal stations in almonds, processing tomatoes, and maize, and 2) evaluate energy balance components on satellite overpass date from the three models to identify causes of deviation and to quantify sources of uncertainty.

2. Materials and Methods

2.1 Model description

Three single-source RS-based ET models (pySEBAL, METRIC and SEBS) were selected for evaluation of ET_a. This section describes the specific algorithms for each model. All three models are based on the surface energy balance. ET_a is calculated based on the acquisition of satellite imagery containing the radiometric information at the satellite overpass time. Thus, instantaneous ET_a

calculations are first conducted and then converted to daily ET_a. Due to the lack of information on the surface resistances related to the evaporative process, the instantaneous latent heat flux from these three RS-based models are all computed as a “residual” of the surface energy balance equation (Kustas et al., 1994; Boegh et al., 2002):

$$\lambda E = R_n - H - G \quad (1)$$

where λE is the instantaneous latent heat flux in the atmosphere boundary layer (W/m^2), R_n is the instantaneous net radiation flux (W/m^2), H is the instantaneous sensible heat flux (W/m^2) and G is the instantaneous soil heat flux (W/m^2). Similarities and differences between these three RS-based ET models are described in the next sections.

2.1.1 pySEBAL

pySEBAL is a version of the SEBAL algorithm that has been developed by Hessels et al. (2017) in Python environment, which is an open source platform that run SEBAL by semi-automatically processing selected Landsat satellite imagery. Both pySEBAL and METRIC use an automated anchor pixel approach in selecting cold and hot pixels. The selection of cold and hot pixels involves setting a predefined criterion and then using computer algorithms to identify the pixels in the image that meet those criteria. The predefined criteria includes assessing ranges in NDVI, Ts, momentum roughness length (z_{om}), and α. R_n is calculated by deducting all outgoing radiation fluxes from all incoming radiation fluxes as:

$$R_n = (1 - \alpha) R_{s\downarrow} + \varepsilon_0 R_{L\downarrow} - \varepsilon_0 \sigma T_s^4 \quad (2)$$

Where $R_{S\downarrow}$ is the incoming shortwave radiation calculated at the satellite overpass time with clear sky conditions (W/m^2), and $R_{L\downarrow}$ is the incoming longwave radiation (W/m^2). α is the surface albedo (-). ε_0 is the surface emissivity estimated by a semi-empirical relationship involving NDVI and Leaf Area Index (LAI), which can be retrieved from the red and near infrared bands.

σ is the Stephen-Boltzman constant as 5.67×10−8 (W/m^2 K^4), and T_s is land surface temperature (composite soil and vegetation radiometric temperature) (K). G is calculated as a fraction of the R_n, and pySEBAL uses the empirical equation of G developed by Bastiaanssen (1995):

$$G = T_{s,datum}(0.0038 + 0.007\alpha)(1 - 0.98 NDVI^4) \times R_n \quad (3)$$

Where $T_{s,datum}$ is the corrected land surface temperature (T_s) based on the DEM of the area of interest (AOI) by considering its slope and aspect. An internal calibration of H is applied in pySEBAL, thus no extra atmospheric correction of T_s is needed. H in pySEBAL is calculated using the bulk aerodynamic resistance equation:

$$H = \frac{\rho \times C_p \times dT}{r_{ah}} \quad (4)$$

where ρ is the air density (kg/m^3), and C_p is the specific heat of air at constant pressure which is 1,004 J/(kg K). r_{ah} is the aerodynamic resistance of heat transfer between z_1 and z_2 (s/m). dT parameter is the temperature difference between two near-surface height (z_1 = 0.1 m and z_2 = 2 m) above the canopy layer *(K)*, which is estimated as a linear function of corrected surface temperature $T_{s,datum}$ (Eq.5), being a major assumption for estimating sensible heat flux (Allen et al., 2005; Bastiaanssen, 1995). The coefficients "*a*" and "*b*" in the Eq.5 are determined iteratively for extreme anchors (cold and hot pixels), thus they are specific for every satellite image or area of interest.

$$dT = a + b \times T_{s,datum} \quad (5)$$

$$a = \frac{dT_{hot} - dT_{cold}}{T_{s,datum,hot} - T_{s,datum,cold}} \quad (6)$$

$$b = \frac{dT_{hot} - a}{T_{s,datum,hot}} \quad (7)$$

In pySEBAL anchor pixels are determined by identify three-pixel populations namely i) cold vegetative pixels, ii) water pixels, and iii) hot pixels. The cold vegetative pixels were automatically identified as those having maximum NDVI in the scene. Water pixels were classified using Top of Atmosphere reflectance bands involving a combination of non-freezing temperature and negative NDVI as described in Jaafar and Ahmad (2019). Ts for cthe cold pixels was selected from the minimum of vegetative and water pixels. Hot pixels were identified as those having NDVI values in the range of 0.03 and 0.2. Detailed conditions applied for the anchor pixel/limit selection in the pySEBAL, METRIC and SEBS are represented in Table 1.

Based on the instantaneous R_n, H and G at the satellite overpass time, the instantaneous evaporative fraction (EF_i) can be calculated (Eq.8) and converted into daily evaporative fraction (EF_{24}) (Eq.9) by using an advection factor Ω, which is used to reduce errors caused by the ET_a increase during the afternoon (Hong et al., 2014):

$$EF_i = \frac{R_n - H - G}{R_n - G} \tag{8}$$

$$EF_{24} = \Omega \times EF_i \tag{9}$$

where Ω is calculated as:

$$\Omega = 1 + 0.985 \times EF_i \times \{\exp[0.08 \times (e_s - e_a)] - 1\} \tag{10}$$

where e_s is the saturated vapor pressure at temperature of the air above the canopy reference height, and e_a is the actual vapor pressure above canopy height. The daily ET_a is then calculated for each pixel in pySEBAL as:

$$ET_{24} = 8.64 \times 10^7 \times \Omega \times EF_i \times \frac{(R\text{¿¿}n24 - G_{24})}{\lambda \times \rho_w}\text{¿} \tag{11}$$

where ET_{24} is the daily ET_a rate of the satellite overpass date (mm/d), and λ is the latent heat of vaporization (J/kg), and ρ_w is the density of water (kg/m^3) (Rwasoka et al., 2011). G_{24} is the daily average soil heat flux (W/m^2), which is assumed as 0 for soil and vegetation surfaces. R_{n24} is the average net radiation of the day (W/m^2), which can be calculated as:

$$R_{n24} = [(1 - \alpha) \times R_a - 110] \times \tau_{sw} \quad (12)$$

Where R_a is the daily extraterrestrial solar radiation (W/m^2). τ_{sw} is the daily atmospheric transmissivity affected by humidity, dust and other pollutants in the air. More details of the algorithm in the pySEBAL can be obtained from Hessels et al. (2017).

2.1.2 METRIC

As a variant of the SEBAL model, the calculation method of instantaneous H and G in METRIC are the same as in pySEBAL, both assume a linear relationship between T_s and dT. However, there are some notable differences 1) METRIC does not assume that $H_{wet} = 0$ and that $\lambda E_{wet} = R_n - G$ at the wet pixel, instead it uses a soil water balance to track soil water content to confirm that at the hot pixel latent heat approaches zero and at the wet pixel latent equals to 1.05*ET_r (hourly alfalfa ET_0 estimated using ASCE Penman-Monteith); 2) cold pixel are typically selected in well irrigated agricultural areas, where the biophysical characteristics (for example crop height and LAI) are similar to the reference crop (alfalfa); and 3) the upscaling of instantaneous to daily ET_a is based on the reference ET fraction. In METRIC the automated anchor pixel selection starts by determining the minimum and maximum temperatures for the 5% quantile of the pixel values of the land surface temperature raster. Then the cold and hot pixel populations are determined by applying conditional selection based on the following surface parameters Ts, α, NDVI, LAI, and z_{om}.

The two models also use similar approaches in estimation of R_{n24}, the only difference being the term τ_{sw}, in which METRIC uses air pressure and water content of atmosphere while pySEBAL uses height above mean sea level.

Based on the calculated R_n, H and G, instantaneous ET_a at each pixel within the AOI at the satellite overpass time can be computed as:

$$ET_{ins} = 3600 \times \frac{R_n - H - G}{\lambda * \rho_\omega} \quad (13)$$

where ET_{ins} is the instantaneous ET_a rate (mm/h). Then the reference evaporative fraction ET_rF is calculated as:

$$ET_r F = \frac{ET_{ins}}{ET_r} \quad (14)$$

where ET_r is the ET_0 of alfalfa per hour (mm/h) at the satellite overpass time, which is usually calculated from meteorological data from a nearby weather station. Assuming a constant daily ET_rF, daily ET_{24} is computed as:

$$ET_{24} = ET_r F \times ET_{r,24} \quad (15)$$

where $ET_{r,24}$ is the cumulative daily ET_r at the satellite overpass date (mm/d), which can be calculated using Penman-Monteith equation (Allen et al., 1998). For more detailed descriptions of algorithms in the METRIC the reader is referred to Allen et al. (2007b). Recently the METRIC model has been written and packaged in R programming language in the “water” package version 0.6 (Olmedo et al., 2017). Similar to pySEBAL, this “water” package also adopted an automated hot/cold pixel selection procedure. In addition, it accepts Level-2 Landsat atmospherically corrected surface reflectance products for Landsat 8 imagery.

2.1.3 SEBS

Just like pySEBAL, SEBS is another commonly used energy balance model for ET_a estimation based on Eq. 1. The main equations constituting the SEBS algorithm are described below for a detailed description of this method the reader is referred Su (2002). The calculations of R_n in SEBS is similar to pySEBAL (Eq.2) except for a slight change in the equation of LAI, which refer to Choudhury (1987). SEBS uses the algorithm by Su (2002) to calculate the G as a function of fractional canopy cover (f_c) as follows:

$$G = R_n \text{¿} \quad (16)$$

where Γ is the soil heat flux ratio with constants of Γ_c=0.05 for full vegetation cover and Γ_c=0.315 for bare soil based on prior work by of Monteith (1973) and Kustas and Daughtry (1990).

SEBS uses Monin–Obukhov similarity theory for pixel by pixel estimation of H using the available energy under dry and wet limit conditions as follows:

$$H = \frac{\rho C_p (\theta_o - \theta_a)}{k u_{\text{¿}} \left[\text{¿} \left(\frac{z - d_o}{z_{oh}} \right) - \Psi_h \left(\frac{z - d_o}{L} \right) + \Psi_h \left(\frac{z_{oh}}{L} \right) \right]} \quad (17)$$

$$u_{\text{¿}} = \frac{uk}{\left[\text{¿} \left(\frac{z - d_o}{z_{om}} \right) - \Psi_h \left(\frac{z - d_o}{L} \right) + \Psi_h \left(\frac{z_{om}}{L} \right) \right]} \quad (18)$$

Where u_* is the friction velocity (m/s), u is the wind speed (m/s), k is the von Karman constant equal to 0.41 (-), d_o is the zero plane displacement height (m), z is height above the evaporating surface (m), z_{oh} is roughness height for heat transfer (m), z_{om} is roughness height for momentum transfer (m). θ_o and θ_a are the potential temperatures at the surface and at height z (K), and Ψ_m and Ψ_h are stability functions based on Brutsaert (1999) (-). L is the Obukhov length (m), for more details on the application of the similarity theory in SEBS the reader is referred to Su (2002). H, initially derived in SEBS at each pixel, is scaled between the sensible heat under dry and wet limits. This scaling method is performed for each pixel within the image after calculating H based on Eq. (1) by considering the λE at the dry and wet limit conditions. At the dry limit, latent heat (λE_{dry}) approaches zero and sensible heat (H_{dry}) reaches its maximum value as shown in equations 19 and 20:

$$\lambda E_{dry} = R_n - G_o - H_{dry} \equiv 0, H_{dry} = R_n - G_o \quad (19)$$

On the other hand, at the wet limit sensible heat (H_{wet}) approaches its minimum values and latent heat (λE_{wet}) occurs at its potential rate as described in equation below:

$$\lambda E_{wet}=R_n-G_o-H_{wet},H_{wet}=R_n-G_o-\lambda E_{wet} \quad (20)$$

At the wet limit, the bulk surface internal resistance approaches zero and H_{wet} can be estimated from Penman-Monteith type combination equation as shown by Su (2002).

The instantaneous evaporative fraction Λ_r is calculated with energy balance at limiting conditions according to Su (2002):

$$\Lambda_r=1-\frac{H-H_{wet}}{H_{dry}-H_{wet}} \quad (21)$$

Assuming the Λ_r to be constant over daily time step, the daily evaporative fraction (Λ_{24}) and daily evapotranspiration (ET_{24}) can thus be computed as:

$$\Lambda_{24}=\frac{\Lambda_r\times\lambda ET_{wet}}{R_n-G} \quad (22)$$

$$ET_{24}=8.64\times10^{7}\times\frac{\Lambda_{24}\times(R\text{¿¿}n24-G_{24})}{\lambda\times\rho_{\omega}}\text{¿} \quad (23)$$

2.2 Study area and data collection

2.2.1 Field experiments

In California, of the over 17.4 million hectares are used for agriculture, about 40% is cropland and the rest is pasture and rangeland. The Central Valley has a Mediterranean climate with winter rainfall and hot summers and high annual evaporative demand ranging from 889 to 1,270 mm (Williams, 2001). This study included fields located on two large commercial farms and one experimental farm in the Central Valley (Fig. 1). From north to south, three fields were planted with maize, processing tomatoes and almonds respectively. As a required input in pySEBAL, soil information of these fields was obtained from USDA NRCS's Web Soil Survey (WSS) with soil texture ranging from fine sandy loam to silty clay (Table 2). Maize and processing tomato fields were irrigated using subsurface drip irrigation, and the almond orchards were irrigated using double line surface drip irrigation with variable rate irrigation (VRI) capabilities for automation. The residual of energy balance approach and surface renewal equipment were used for the actual crop water use (ET_a) measurements. Tule Technologies systems (www.tuletechnologies.com) were installed in these three fields to measure daily ET_a for almonds (May 11th of 2018 to May 13th of 2019), processing tomatoes (May 9th to August 18th of 2018) and maize (May 24th to September 5th of 2018). The Tule surface renewal stations consist of a thin fine wire thermocouple placed about 3.3 feet above the crop canopies to estimate sensible heat H, and use spatially distributed R_n from the GOES satellite in evaluation of the energy balance. Daily G value is assumed negligible when compared to R_n, H and λE. According to the measurement principle of Tule sensor, the yellow rectangle in Fig.1 represents the approximate measurement zone of each monitoring point given what we know about the prevailing wind direction and the wind fetch length at the sensor height. The measured ET values are more or less representative of this measurement area. Data is transmitted through telemetry and the farmer access it through the web from this url https://www.tuletechnologies.com/.

2.2.2 Remote sensing based evapotranspiration model inputs

(1) Remote sensing data

With clear sky conditions permitting, a total of 27 Landsat 8 OLI/TIRS images (20 Path 42/Row35 images for the almond field, 7 Path 44/Row 33 images for processing tomato and maize fields) were obtained from the USGS Earth Resources Observation and Science Center (http://eros.usgs.gov/) for the 2018-2019 growing season. The imagery acquisition dates for almond, processing tomato and maize fields are presented in Table 3, in which tomato and maize fields were located within the range of one Landsat 8 imagery. Three 90 m high-resolution Shuttle Radar Topography Mission (SRTM) - digital elevation model (DEM) maps for these fields were downloaded from the USGS

EROS Center. They were then clipped to the size of the study area to shorten the computation time in pySEBAL. All the preprocessing of images were conducted with QGIS and ArcGIS. Based on empirical equations, DEM, meteorological and soil data, Landsat imagery were processed with atmospheric correction automatically performed in pySEBAL and METRIC ("water" package version 0.6). SEBS model was run in python environment.

(2) Meteorological data

Three nearest automated weather stations from the California Irrigation Management Information System (CIMIS) (Table 4) provided the hourly and daily meteorological data such as relative humidity, wind speed, solar radiation and air temperature required for ET_a estimation in pySEBAL, SEBS and METRIC in this study.

2.3 Validation of ET_a simulated by RS-based models

RS-based ET models generated spatial ET_a (mm/d) from instantaneous latent heat flux for each of the input satellite images. To reconstruct the time series of daily ET_a and compare them with daily Tule-based ET_a throughout the growing season, RS-based daily ET_a values were interpolated between two adjacent satellite overpasses using the ET_0 from the nearest weather station and the linear interpolated evaporative fraction. ET_0 was estimated using the CIMIS Penman–Monteith equation (Doorembos and Pruitt, 1977) with hourly data of solar radiation, wind speed, air temperature and relative humidity from the nearest CIMIS weather station for each study field (Table 4). The estimated ET_a values from three RS-based models were compared with surface renewal generated ET_a from Tule Sensors at the three field sites. The area of each measurement zone equals to that of several remote sensing pixels (one pixel is 30×30m), thus the Tule-based ET_a can represent the average ET_a of whole measurement zone including several pixels (Fig.1). We took advantage of ArcGIS to calculate the average of RS-based ET_a within the range of each measurement zone and compared it with Tule-based ET_a to see the model performance.

Statistical goodness of fit measures used in this study included the Root Mean Square Error (RMSE), Nash-Sutcliffe efficiency (NSE) and correlation coefficient (R^2). For an overview of goodness of fit measures typically used in hydrology, the reader is referred to (Legates and McCabe, 1999).

3. Results and Discussion

3.1 Comparing remote sensing based evapotranspiration estimates to surface renewal measurements

Comparison of the estimated and measured daily ET_a values are shown in Fig.2. Since the goal of comparing these RS-based ET models is to estimate daily ET_a for irrigation scheduling, more focus was put on the RMSE between the model estimates and Tule measurements. For almonds, the performance of all the three RS-based ET models (pySEBAL, METRIC and SEBAL) was good with RMSE ranging from 0.9 mm/d to 1.6 mm/d, NSE ranged from 0.68 to 0.77, and R^2 ranged from 0.74 to 0.82. For processing tomatoes, SEBS performed best (RMSE = 0.6 mm/d, NSE = 0.66 and R^2= 0.86) while pySEBAL (RMSE = 1.79 mm/d, NSE = 0.06 and R^2=0.37) and METRIC (RMSE = 1.78, NSE= 0.11 and R^2 = 0.41) performed poorly during the growing season due to the underestimation of daily ET_a. For maize, overestimations were observed in all three RS-based models, among which SEBS performed better (RMSE = 1.0 mm/d, NSE = 0.46 and R^2= 0.74) than pySEBAL (RMSE=1.08 mm/d, NSE = 0.43 and R^2 = 0.72) and METRIC (RMSE = 1.2 mm/d, NSE = 0.4 and R^2 = 0.78). Fig.3 shows the time-series daily ET_a for the almond orchard (VRI and control blocks), processing tomato, and maize fields generated using pySEBAL, METRIC, SEBS, Tule measurements, and FAO-56 methodology. Mean daily ET_a from pySEBAL, METRIC, and SEBS were 5.6, 6.5, and 4.9 mm/d during the almond growing season and 2.1, 2.6, and 2.4 mm/d during the dormant season. Compared to the mean Tule measurements, it was determined that the average values of pySEBAL, METRIC, and SEBS's estimates were respectively 26%, 36%, and 11% higher during the almond growing season (May 11th 2018 to October 31th 2018) and 4%, 1% and 7% higher during the dormant season (November 1st 2018 to February 28th 2019) and part of the growing season before full coverage (March 1st 2019 to May 13th 2019). The overestimations of daily ET_a were likely from the warmer cold/wet pixels selected within the well-watered farmland. Long et al. (2011) and Lian and Huang (2016) reported that a warmer cold pixel selection in the initial stages of the growing season might lead to a decrease in estimated H and an increase in estimated ET_a. Because when the vegetation fraction was relatively low at during initial growth stages, a cold extreme pixel selected from irrigated farmland rather than from a water body might not meet the potential ET requirement. They also found that the continuous linearly interpolated daily ET_a between two clear-day ET_a may be higher than daily ET_a when cloudy-days exist in this period.

For processing tomatoes, mean daily ET_a from pySEBAL, METRIC, and SEBS during the growing season were 4.1, 4.3, and 4.9 mm respectively, which were 22%, 19%, and 7% respectively less than mean Tule measurements. The underestimation of pySEBAL and METRIC models for the tomato field during the early stage of crop growth (from May 9th to June 26th) may be attributed to small vegetation cover early in the season. As a single-source model, if a large portion of the soil is exposed and water stress conditions occur early in the season, both G and H may be large and errors in the two energy balance components will significantly affect the instantaneous λE. With full vegetation cover at the medium-late growth stages, H is usually small and λE is not substantially affected by H even if the sensible heat flux is not accurately estimated. Some researchers also reported underestimations of ET_a using SEBAL and METRIC models for crop's initial growth stages with low vegetation coverage and water stress conditions (Mcebisi et al., 2015; Allen et al., 2011). With regards to METRIC, using a constant ET_rF to estimate daily ET_a may result in underestimation of water stress conditions (Allen et al., 2011). Compared to the Tule estimates and SEBS, the underestimation of daily ET_a by pySEBAL and METRIC may also be attributed to the underestimated daily average net radiation calculated by empirical equations when upscaling instantaneous ET_a to daily ET_a. The use of empirical formula for daily average net radiation in pySEBAL when upscaling the instantaneous ET_a to daily ET_a may not work on cloudy days. Applying either measured or modeled daily net radiation for upscaling instantaneous ET_a could reduce the errors in daily ET_a estimation (Olmedo et al., 2017). Some previous studies also reported the need for calibrating the empirical equation of daily average net radiation to account for local atmospheric conditions to improve the daily ET_a estimation (Zhang et al., 2013; Ramesh and Gabriel, 2015). For maize, most of the RS-based ET models were above the 1:1 line indicating they overestimated ET_a. The pySEBAL, METRIC and SEBS-based mean daily ET_a were 6.4, 5.8, and 5.1 mm/d, overestimating daily ET_a by 31%, 26%, and 12%, respectively.

Overall, when using surface renewal estimates from Tule as a reasonable reference (although we acknowledge there is level of measurement uncertainty with this method), SEBS model performed better than both pySEBAL and METRIC with lower RMSE and higher R^2 and NSE for the time-series ET_a estimations of almonds, processing tomatoes, and maize at the field scale. This suggests that SEBS could improve the spatiotemporal ET_a estimation over orchards or field crops, because the SEBS model is more sensitive to the influence of differences in underlying surface characteristics on the resistance to heat transfer (Gao and Long, 2008; Verhoef et al., 1997). Many researchers have reported that SEBS performance was better than METRIC and SEBAL for ET_a estimation (Gowda et al., 2013; Wagle et al., 2017; Bhattarai et al., 2016; Paul, 2013). In addition, as pySEBAL, METRIC, and SEBS all used reference ET approach to reconstruct time-series of daily ET_a between cloud free days, the cloudy-day evaporative fraction (*EF* or ET_rF) can be linearly interpolated based on two nearby clear-day ET_rF, which is similar to generating seasonal K_c with two K_c values of two days. Thus, the calculation of instantaneous ET_a and different approaches embedded in different RS-based models used for upscaling instantaneous ET_a to daily ET_a were the main cause of bias in time-series daily ET_a estimates.

3.2 Inter-comparison of daily evapotranspiration estimations among three RS-based models

The inter-comparisons of interpolated daily ET_a estimates from pySEBAL, METRIC, and SEBS were performed as density plots (Fig. 4) to examine the applicability and limitation of these models. The period of comparison was for almonds (May 11th of 2018 to May 13th of 2019), processing tomatoes (May 9th to August 18th of 2018) and maize (May 24th to September 5th of 2018. It is shown that there was some degree of linearity for ET_a estimates from pySEBAL and METRIC and SEBS for almond and maize. For processing tomato, the relationship between daily pySEBAL and METRIC based ET_a was in good agreement, while poor linearity existed between pySEBAL and METRIC with SEBS (Fig.4b). The big variation was caused by the smaller daily ET_a estimates from pySEBAL and METRIC than SEBS during the early growth stages of processing tomato. To better understand the possible source for variations in the density plot involving three RS-based models, we presented comparison of modelled fluxes for three RS-based models in Fig. 5. As we mentioned before that R_n used by Tule is modeled from GOES satellite and on a daily time scale *G* is zero in Tule. *H* is the only measured energy balance component from Tule Sensors, thus we also include the comparison of measured *H* from Tule with simulated *H* from RS-based models in Fig.5. As there were similar values of energy fluxes between two adjacent almond fields with different irrigation management, only simulated energy balance components of the almond field applied with VRI are presented in this paper.

Compared to METRIC and SEBS, R_n was underestimated by pySEBAL for the whole growing season for all three crops, which could be one of the main reasons of the smaller daily ET_a simulated by pySEBAL in Fig. 4a. The simulated G were relatively consistent among these three RS-based models, especially for the almond field (Fig.5). For the simulation of H, SEBS performed much better than pySEBAL and METRIC when compared to Tule measured H. pySEBAL and METRIC generated greater values than SEBS for these three crops on all satellite overpass dates, and relatively low Tule measured H for three crops indicated that they were almost at the potential evapotranspiration rate during their growing seasons. All three crop sites were well irrigated during the growing season in this study, which matched with the Tule measured H estimation results. The biases between estimated and measured H were ranked in the order of processing tomato > maize > almond. Simulation results showed similar performances of H estimates for almond among three models, while H estimates for processing tomato varied greatly among three models. As described above, derivation of H in pySEBAL and METRIC relies on the presence of extreme T_s (cold and hot or wet and dry) pixels in the imagery. Especially for small areas, for homogeneous land-use types, or for imagery with low-moderate resolutions, the assumption that all possible extreme cold and hot endmembers of a landscape are presented within the image might be not valid. In other words, lack of presence of high water use crops (full vegetation or water-sufficient vegetation and soil) in the imagery may result in considerable errors in the estimation of H. In contrast to contextual models, single-pixel methods (SEBS) estimate ET for each pixel independently from all other pixels in the image by solving the surface energy balance equation. Besides, with less simulated R_n - G, pySEBAL and METRIC partitioned less available energy into H and λE. Poor performance and underestimation of λE by pySEBAL and METRIC for processing tomatoes was exactly because of the overestimation of *H*, which can be attributed to the low vegetation coverage and water stress conditions in the early growth stages.

To improve the definition of the cold and hot anchor pixels in two contextual models (pySEBAL and METRIC), high resolution imagery such as UAS TIR imagery would be particularly suitable for routine application in contextual RS-based ET models. However, due to the restriction of practical considerations including battery life and the need for high imagery overlap as well as the requirement of concerning the visibility of the UAS during operation, the applicability of high resolution UAS TIR imagery is under development.

4. Conclusions

The performance of three widely used single-source surface energy balance remote sensing ET models (pySEBAL, METRIC, and SEBS) were evaluated aganist surface renewal measurements in almond, processing tomato, and maize in California's Central Valley during the 2018-2019 growing season. Based on combined scores from RMSE, NSE and R^2, performance of the three RS-based ET models were ranked in the order of SEBS> pySEBAL> METRIC to estimate daily ET_a. Our results showed that pySEBAL, METRIC, and SEBS could provide resaonable ET estimates for almond, processing tomato, and maize during the growing season, except for the underestimation of pySEBAL and METRIC-based ET_a estimates during early growth stages of processing tomatoes. Thus, they could be used in precision agriculture decision support tools for simulating daily ET_a and provide information for optimizing irrigation management. Using site-specific ET_a estimates from RS based models such as SEBS could have a huge impact on water use in agriculture given the large acreage of almonds in California. Performances of pySEBAL and METRIC in early growth stages of processing tomato indicated their limitation in daily ET_a estimation in the early growth stage (low vegetation coverage and water stress condition) and their usefulness after full canopy closure. For cropped surfaces such as an orchard or row-crop field, SEBS can provide a better estimation of ET_a than pySEBAL and METRIC. This study provided new information on potential applicability of remote sensing based ET models for guiding irrigation management at the field scale.

Acknowledgements

This study was supported by the USDA Specialty Crop Block Grant Program from Almond Board of California [grant number 180001083SC], Foundation for Food and Agricultural Research [grant number 430871] and the International Postdoctoral Exchange Fellowship Program from the Office of China Postdoctoral Council [grant number 20180044]. Special thanks also go to the technical support received from Ernie Wilson from the Tule Technologies Inc. team to provide information and data.

Reference

Allen, R., Irmak, A., Trezza, R., Hendrickx, J. M. H., Bastiaanssen, W., Kjaersgaard, J., 2011a. Satellite-based ET estimation in agriculture using sebal and metric. Hydrological Processes, 25(26), 4011-4027.

Allen, R.G., Tasumi, M., Morse, A., Trezza, R., 2005. A Landsat-based energy balance and evapotranspiration model in Western US water rights regulation and planning. Irrig. Drain. Syst. 19, 251–268.

Allen, R. G., Pereira, L. S., Howell, T. A., Jensen, M. E., 2011b. Evapotranspiration information reporting: ii. Recommended documentation. Agricultural Water Management, 98(6), 921-929.

Allen, R.G., Pereira, L.S., Raes, D., Smith, M., 1998. Crop evapotranspiration. Guidelines for computing crop water requirements. In: FAO Irrigation and Drainage Paper No. 56. Rome, Italy.

Allen, R.G., Tasumi, M., Morse, A., Trezza, R., Wright, J., Bastiaanssen, W.G.M.,Kramber, W., Lorite, I., Robison, C., 2007a. Satellite-based energy balance for Mapping Evapotranspiration with Internalized Calibration (METRIC)—applications. Journal of Irrigation and Drainage Engineering. 133, 395–406.

Allen, R.G., Tasumi, M., Trezza, R., 2007b. Satellite-based energy balance for Mapping Evapotranspiration with Internalized Calibration (METRIC)—model. Journal of Irrigation and Drainage Engineering. 133, 380–394.

Allen, R. G., Trezza, R., Tasumi, M., 2006. Analytical integrated functions for daily solar radiation on slopes. Agricultural and Forest Meteorology, 139 (1), 55-73.

Allen, R. G., Trezza, R., Kilic, A., Tasumi, M., Li, H., 2013. Sensitivity of Landsat-scale energy balance to aerodynamic variability in mountains and complex terrain. JAWRA Journal of the American Water Resources Association, 49(3), 592-604.

Anderson, M. C., Norman, J. M., Kustas, W. P., Houborg, R., Starks, P. J., Agam, N., 2008. A thermal-based remote sensing technique for routine mapping of land-surface carbon, water and energy fluxes from field to regional scales. Remote Sensing of Environment, 112(12), 4227-4241.

Bastiaanssen, W., 1995. Regionalization of Surface Flux Densities and Moisture Indicators in Composite Terrain: a Remote Sensing Approach under Clear Skies in Mediterranean Climates. SC-DLO.

Bastiaanssen, W. G. M., Menenti, M., Feddes, R. A., Holtslag, A. A. M., 1998. A remotesensing surface energy balance algorithm for land (SEBAL) 1. Formulation. Journl of Hydrology. 212, 198–212.

Bastiaanssen, W. G. M., Mobin-ud-Din Ahmad, Chemin, Y., 2002. Satellite surveillance of evaporative depletion across the Indus basin. Water Resources Research, 38(12).

Bastiaanssen, W. G. M., Noordman, E. J. M., Pelgrum, H., Davids, G., Thoreson, B. P., Allen, R. G., 2005. SEBAL Model with Remotely Sensed Data to

Improve Water-Resources Management under Actual Field Conditions. Journal of Irrigationa and Drainage Engineering. 121, 1.

Bhattarai, N., Quackenbush, L. J., Im, J., Shaw, S. B., 2017. A new optimized algorithm for automating endmember pixel selection in the sebal and metric models. Remote Sensing of Environment, 196, 178-192.

Bhattarai, N., Shaw, S. B., Quackenbush, L. J., Im, J., Niraula, R., 2016. Evaluating five remote sensing based single-source surface energy balance models for estimating daily evapotranspiration in a humid subtropical climate. International Journal of Applied Earth Observation & Geoinformation, 49, 75-86.

Bisht, G., Venturini, V., Islam, S., Le, J., 2005. Estimation of the net radiation using modis (moderate resolution imaging spectroradiometer) data for clear sky days. Remote Sensing of Environment, 97(1), 52-67.

Beljaars, A.C.M., Holtslag, A.A.M., 1991. Flux parameterization over land surfaces for atmospheric models. J. Appl. Meteorol. 30 (3), 327–341.

Carlson, T., 2007. Anoverview of the "Triangle Method" for estimating surface evapotranspiration and soil moisture from satellite imagery, Sensors, 7(8), 1612–1629.

Choudhury, B. J., 1987. Relationships between vegetation indices, radiation absorption, and net photosynthesis evaluated by a sensitivity analysis. Remote Sensing of Environment, 22 (2), 209-233.

CDFA, 2018. California Agricultural Statistics Review 2017–2018. California Department of Food and Agriculture, Sacramento, CA, USA.

Doorenbos, J., Pruitt, W. O., 1977. Crop water requirements. FAO Irrigation and Drainage Paper No. 24, Food and Agriculture Organization, Rome, Italy.

Evett, S.R., Kustas, W.P., Gowda, P.H., Anderson, M.C., Prueger, J.H., 2012. Overview of the Bushland Evapotranspiration and Agricultural Remote Sensing Experiment 2008(BEAREX08): a field experiment evaluating methods for quantifying ET at multiple scales Adv. Water Resour., 50

(2012), pp. 4-19

Fulton, A. E., Little, C. C., Snyder, R. L., Lampinen, B. D., Buchner, R. P., 2017. Evaluation of Crop Coefficients and Evapotranspiration in English Walnut. In 2017 ASABE Annual International Meeting (p.1). American Society of Agricultural and Biological Engineers.

Gao, Y.C., Long, D., 2008. Intercomparison of remote sensing-based models for estimation of evapotranspiration and accuracy assessment based on swat. Hydrological Processes, 22(25), 4850-4869.

Gowda, P. H., Howell, T. A., Paul, G., Colaizzi, P. D., Marek, T. H., Su, B., 2013. Deriving hourly evapotranspiration rates with SEBS: a lysimetric evaluation. Vadose Zone Journal, 12(3).

Hanson, B., May, D., 2006. New crop coefficients developed for high-yield processing tomatoes. California Agriculture, 60(2), 95-99.

Hessels, T., van Opstal, J., Trambauer, P., Bastiaanssen, W., Faouzi, M., Mohamed, Y., ErRaji, A., 2017. pySEBAL version 3.3.7.

Hong, S. H., Hendrickx, J. M. H., Kleissl, J., Allen, R. G., Steinwand, A. L., 2014. Evaluation of an extreme-condition-inverse calibration remote sensing model for mapping energy balance fluxes in arid riparian areas. Hydrology and Earth System Sciences Discussions, 11(12), 13479-13539.

Hu, Y.G., Buttar, N. A., Tanny, J., Snyder, R. L., Savage, M. J., Lakhiar, I. A., 2018. Surface renewal application for estimating evapotranspiration: A review. Advances in Meteorology, 1-13.

Jaafar, H. H., Ahmad, F. A., 2019. Time series trends of Landsat-based ET using automated calibration in METRIC and SEBAL: The Bekaa Valley, Lebanon. Remote Sensing of Environment. In press.

Jiang, L., Islam, S., 1999. A methodology for estimation of surfaceevapotranspiration over large areas using remote sensing observations. Geophysical Research Letters, 26(17), 2773-2776.

Khan, S. I., Hong, Y., Vieux, B., Liu, W. J., Tang, Q., Durand, M., et al., 2010.

Development and evaluation of an actual evapotranspiration estimation algorithm using satellite remote sensing and meteorological observational network in Oklahoma. International Journal of Remote Sensing, 31(14), 3799-3819.

Kustas, W.P., Daughtry, C.S.T., 1990. Estimation of soil heat flux/net radiation ratio from spectral data. Agric. Forest Meteorol. 49 (3), 205–223.

Kyaw, T. P. U., Qiu, J., SUN, H., Watanabe, T., Brunet, Y., 1995. SURFACE RENEWAL ANALYSIS-A NEW METHOD TO OBTAIN SCALAR FLUXES. Agricultural and Forest Meteorology, 74(1-2), 119-137.

Legates, D. R., and McCabe Jr., G. J., 1999. Evaluating the Use of "Goodness-of-Fit" Measures in Hydrologic and Hydroclimatic Model Validation. Water Res. Research, 35(1), 233-241.

Li, Z. L., Tang, R. L., Wan, Z. M., Bi, Y. Y., Zhou, C. H., Tang, B. H., Yan G. J., Zhang, X. Y., 2009. A review of current methodologies for regional evapotranspiration estimation from remotely sensed data. Sensors, 9(5), 3801-3853.

Lian, J., Huang, M., 2016. Comparison of three remote sensing based models to estimate evapotranspiration in an oasis-desert region. Agricultural Water Management, 165, 153-162.

Long, D., Longuevergne, L., Scanlon, B. R., 2014. Uncertainty in evapotranspiration from land surface modeling, remote sensing, and grace satellites. Water Resources Research, 50 (2), 1131–1151.

Long, D., Singh, V. P., 2012. A two-source trapezoid model for evapotranspiration (TTME) from satellite imagery, Remote Sens. Environ., 121, 370–388.

Long, D., Singh, V. P., Li, Z. L., 2011. How sensitive is SEBAL to changes in input variables, domain size and satellite sensor? J. Geophys. Res. Atmos. 116, D21107.Mancosu, N., Snyder, R., Kyriakakis, G., & Spano, D., 2015. Water scarcity and future challenges for food production. Water, 7 (3), 975-992.

Mcebisi, M., Chávez José, Allan, A., 2015. SEBAL-a: a remote sensing ET algorithm that accounts for advection with limited data. Part I: development and validation. Remote Sensing, 7 (11), 15046-15067.

Mengistu, M. G., Savage, M. J., 2010. Surface renewal method for estimating sensible heat flux. Water SA, 36(1).

Mohamed, Y. A., Bastiaanssen, W. G. M., Savenije, H. H. G., 2004. Spatial variability of evaporation and moisture storage in the swamps of the upper Nile studied by remote sensing techniques. Journal of Hydrology, 289(1-4), 0-164.

Montazar, A., Bali, K., Zaccaria, D., Putnam, D., 2018. Viability of subsurface drip irrigation for alfalfa production in the low desert of California. In 2018 ASABE Annual International Meeting (p. 1). American Society of Agricultural and Biological Engineers.

Monteith, J.L., 1973. Principles of Environmental Physics. Edward Arnold Press.

Norman, J. M., Kustas, W. P., Humes, K. S., 1995. Source approach for estimating soil and vegetation energy fluxes in observations of directional radiometric surface temperature. Agricultural and Forest Meteorology, 77(3-4), 263-293.

Mu, Q., Zhao, M., Running, S. W., 2011. Improvements to a MODIS global terrestrial evapotranspiration algorithm. Remote sensing of environment, 115(8), 1781-1800.

Nyolei, D., Nsaali, M., Minaya, V., Griensven, V. A., Mbilinyi, B., Diels, J., Hessels, T., Kahimba, F., 2019. High resolution Mapping of Agricultural Water Productivity using SEBAL in a cultivated African Catchment, Tanzania. Physics and Chemistry of the Earth, in Press.

Olmedo, G.F., Ortega-Farias, S., Fonseca-Luengo, D., de la Fuente-Saiz, D., Peñailillo, F.F., 2017. Water: actual evapotranspiration with energy balance models. In: R Package Version 0.6.

Paul, G., 2013. Evaluation of surface energy balance models for mapping evapotranspiration using very high resolution airborne remote sensing data. Dissertations & Theses - Gradworks.

Payero, J., Harris, T., 2010. Evaluation of the surface renewal method to estimate crop evapotranspiration of a cotton field. In "Food Security from Sustainable Agriculture", Proceedings of the 15th Australian Agronomy Conference, 15-18 November 2010, Lincoln, New Zealand. Australian Society of Agronomy Inc.

Ramesh, S., Gabriel, S., 2015. Comparison of four different energy balance models for estimating evapotranspiration in the Midwestern United States. Water, 8(1), 9.

Rango, A., 1994. Application of remote sensing methods to hydrology and water resources. International Association of Scientific Hydrology. Bulletin, 39(4), 12.

Rieger, T., 2017. Developments in vineyard mechanisation and precision management. Australian and New Zealand Grapegrower and Winemaker, (639), 65.

Rosa, R., Dicken, U. , Tanny, J., 2013. Estimating evapotranspiration from processing tomato using the surface renewal technique. Biosystems Engineering, 114(4), 406-413.

Rwasoka, D. T., Gumindoga, W. & Gwenzi, J. Estimation of actual ET using the Surface Energy Balance System (SEBS) algorithm in the Upper Manyame catchment in Zimbabwe. Phys. Chem. Earth. 36, 736–746 (2011).

Sanchez, L. A., B. Sams, M. M. Alsina, N. Hinds, L. J. Klein and N. Dokoozlian. 2017. Improving vineyard water use efficiency and yield with variable rate irrigation in California. Advances in Animal Biosciences: Precision Agriculture (ECPA) 2017, 8:2, pp 574–577

Senay, G. B., Budde, M., Verdin, J. P., Melesse, A. M., 2007. A coupled remote sensing and simplified surface energy balance approach to estimate actual evapotranspiration from irrigated fields. Sensors, 7(6), 979-1000.

Senay, G. B., Friedrichs, M. K., Singh, R. K., Velpuri, N. M., 2016. Evaluating landsat 8 evapotranspiration for water use mapping in the Colorado river basin. Remote Sensing of Environment, 185, 171-185.

Shapland, T. M., Snyder, R. L., Smart, D. R., Williams, L. E., 2012. Estimation of actual evapotranspiration in winegrape vineyards located on hillside terrain using surface renewal analysis. Irrigation Science, 30, 471–484.

Simmons, L. J., Wang, J., Sammis, T. W., Miller, D. R., 2007. An evaluation of two inexpensive energy-balance techniques for measuring water use in flood-irrigated pecans (carya illinoinensis). Agricultural Water Management, 88(1), 181-191.

Snyder, R. L., Lanini, B. J., Shaw, D. A., Pruitt, W. O., 1987a. Using reference evapotranspiration (ET_0) and crop coefficients to estimate crop evapotranspiration (ET_c) for trees and vines. Leaflet - University of California.

Snyder, R. L., Lanini, B. J., Shaw, D. A., Priott, W. O., 1987b. Using reference evapotranspiration (ET_0) and crop coefficients to estimate crop evapotranspiration (ET_c) for agronomic crops, grasses, and vegetable crops. Leaflet - University of California, Cooperative Extension Service (USA).

Snyder, R. L., Spano, D., Duce, P., Paw, U. K. T., Rivera, M., 2008. Surface renewal estimation of pasture evapotranspiration. Journal of Irrigation & Drainage Engineering, 134(6), 716-721.

Spano, D., Snyder, R. L., Duce, P., K., T. P. U., 2000. Estimating sensible and latent heat flux densities from grapevine canopies using surface renewal. Agricultural & Forest Meteorology, 104(3), 171-183.

Sugita, M., Brutsaert, W., 1991. Daily evaporation over a region from lower boundary layer profiles measured with radiosondes. Water Resources Research, 27(5), 747-752.

Su, Z. B., 2002. A surface energy balance system (sebs) for estimation of turbulent heat fluxes from point to continental scale.

Tasumi, M., Kimura, R., 2013. Estimation of volumetric soil water content over the liudaogou river basin of the loess plateau using the swest method with spatial and temporal variability. Agricultural Water Management, 118(2), 22-28.

UNESCO-IHE, 2018. pySEBAL.

USDA, 2018. USDA Irrigation and Water Management Survey.

Verhoef, A., De Bruin, H. A. R., & van den Hurk, B. J. J. M. (1997). Some practical notes on the parameter kb1 for sparse vegetation. Journal of Applied Meteorology, 36(1997), 560-572.

Wagle, P., Bhattarai, N., Gowda, P. H., Kakani, V. G., 2017. Performance of five surface energy balance models for estimating daily evapotranspiration in high biomass sorghum. ISPRS Journal of Photogrammetry and Remote Sensing, 128, 192-203.

Wang, K., Dickinson, R. E., 2012. A review of global terrestrial evapotranspiration: observation, modeling, climatology, and climatic variability. Reviews of Geophysics, 50(2), -.

Whitfield, D. M., O'Connell, M. G., Mcallister, A., Mcclymont, L., Sheffield, K., 2011. Sebal-metric estimates of crop water requirement in horticultural crops grown in se Australia. Acta horticulturae, 922(922), 141-148.

Williams, L.E. 2001. Irrigation of wine grapes in California. Practical Winery and Vineyard. November/December.

van den Hurk, B. J. J. M., Holtslag, A. A. M., 1997. On the bulk parameterization of surface fluxes for various conditions and parameter ranges. Boundary-Lay. Meteorol. 82 (1), 119–133.

Xiong, Y. J., Zhao, S. H., Tian, F., Qiu, G. Y., 2015. An evapotranspiration product for arid regions based on the three-temperature model and thermal remote sensing. Journal of Hydrology, 530, S0022169415007337.

Zhang, R. H., Sun, X. M., Wang, W. M., Xu, J. P., Zhu, Z. L., Tian, J., 2005. An operational two-layer remote sensing model to estimate surface flux in regional scale: Physical background. Sci. China Ser. D, 48(S1), 225-244.

Zhang, X., Wu, J., Wu, H., Chen, H., Zhang, T., 2013. Improving temporal extrapolation for daily evapotranspiration using radiation measurements. Journal of Applied Remote Sensing, 7(1), 073538.

Zhao, L., Xia, J., Xu, C., Wang, Z., Sobkowiak, L., Long, C., 2013. Evapotranspiration estimation methods in hydrological models. J. Geograph. Sci., 23 (2), 359-369

Zaccaria, D., Carrillo-Cobo, M. T., Montazar, A., Putnam, D. H., & Bali, K. (2017). Assessing the viability of sub-surface drip irrigation for resource-efficient alfalfa production in central and southern California. Water, 9(11), 837.

Table Captions

Table 1. Conditions applied for the hot (dry)/cold (wet) pixel selection in the pySEBAL, METRIC and SEBS.

Table 2. Summary of locations, size and soil types for three observation fields

Table 3. List of near-cloud free Landsat imageries used for ET estimation.

Table 4. Locations of selected nearest California Irrigation Management

Information System (CIMIS) weather stations

Table 1. Conditions applied for the hot (dry)/cold (wet) pixel selection in the pySEBAL, METRIC and SEBS.

pySEBAL			METRIC			SEBS		
Variable	Cold pixel	Hot pixel	Variable	Cold pixel	Hot pixel	Variable	wet pixel	dry pixel
T_s	<Mean_Cold_Pixels + Cold_Pixel_Constant * Diff_Hot_Cold	Mean_Hot_Pixels + Hot_Pixel_Constant * Diff_Hot_Cold	T_s	<Tmin+ ΔT	>Tmax- ΔT	H	$\frac{-\rho C_p}{\gamma_{ew}} \frac{e_s - e}{\gamma}$ ¿/	R_n-G_0
Water_mask	Yes	-	albedo	0.18-0.25	0.13-0.15			

NDVI	-	0.03-0.25	NDVI	0.76-0.84	0.10-0.28	
LAI	-	-	LAI	3-6	-	
Slope	-	0-10%	Zom	0.03-0.08	≤0.005	

Note: Mean_Cold_Pixels = mean temperature of all pixels defined as water; Mean_Hot_Pixels = mean temperature of all pixels defined as hot pixel (due to selection using NDVI and slope); Cold_Pixel_Constant = defined in your excel sheet, and default is 2; hot_Pixel_Constant = defined in your excel sheet, and default is 0.5; Diff_Hot_Cold = Mean_Hot_Pixels - Mean_Cold_Pixels; Calculation method of H_{wet} in SEBS refers to Su (2002).

Table 2. Summary of locations, size and soil types for three observation fields

Field	Location	Elevation	Size of field	Pixel numbers	Soil type	Field capacity (%)	Wilting point (%)
Almond	(37.15°N, 119.53°W)	12m	28.4 hectares (760m*374m)	264	Nord fine sandy loam	22.9	9.9
Processing tomato	(38.53°N, 121.77°W)	15m	1.9 hectares (240m*80m)	14	Yolo silty loam	30.6	16.4
Maize	(36.23°N, 119.45°W)	77m	25.2 hectares (870m*290m)	224	Capay silty clay	34.5	25.7

Table 3. List of near-cloud free Landsat imageries used for ET_a estimation.

Crop field	Image acquisition dates (Year	Landsat type	Sensor

	DOY)		
Almond field	2018 90	8	OLI
	2018 122	8	OLI
	2018 138	8	OLI
	2018 154	8	OLI
	2018 170	8	OLI
	2018 186	8	OLI
	2018 202	8	OLI
	2018 218	8	OLI
	2018 234	8	OLI
	2018 250	8	OLI
	2018 266	8	OLI
	2018 282	8	OLI
	2018 298	8	OLI
	2018 314	8	OLI
	2018 346	8	OLI
	2018 362	8	OLI
	2019 13	8	OLI
	2019 77	8	OLI
	2019 109	8	OLI
	2019 125	8	OLI
Processing tomato and maize fields	2018 104	8	OLI
	2018 152	8	OLI
	2018 168	8	OLI
	2018 184	8	OLI
	2018 200	8	OLI
	2018 216	8	OLI
	2018 232	8	OLI

Table 4. Locations of selected nearest California Irrigation Management Information System (CIMIS) weather stations

Station	Station ID	Crop	Latitude	Longitude	CIMIS Region
Stratford	15	Almond	36.16°N	119.85° W	San Joaquin Valley
Davis	6	Processing tomato	38.54°N	121.78° W	Sacramento Valley
Williams	250	Maize	39.21°N	122.17° W	Sacramento Valley

Figure Captions

Fig. 1 Locations of field sites in the Central Valley of California. Orange point marks indicate locations of Tule surface renewal stations and the yellow rectangles represent the ET_a measurement areas of the Tule sensors, note that the almond orchard had an experiment of VRI (variable rate irrigation) versus control. Note that the size of ET measurement area are 207m*65m for maize field, 105m*67m for processing tomato and 167m*88m*2 for almond field.

Fig. 2. Comparison of the estimated daily ET_a from the pySEBAL, METRIC, and SEBS models and measured daily ET_a from surface renewal method in almond (a, b, c), processing tomato (d, e, f) and maize (g, h, i).

Fig. 3. Time series of daily ET_a based on three RS-based models (pySEBAL, METRIC, and SEBS) and surface renewal (Tule) for the (a-b) almond, (c) processing tomatoes and (d) maize field sites. Daily RS-based ET_a values were linearly interpolated between two satellite overpass dates.

Fig. 4. Density plots of pairwise comparison of estimated daily ET_a using three RS-based ET models for (a) almond, (b) processing tomatoes and (c) maize. Note that different colors in the density plots refer to the frequency of data points at each location, with red for low frequency and blue for high frequency.

Fig. 5. Boxplots of inter-comparison of simulated instantaneous energy balance fluxes (R_n, G, H and LE) using three RS-based ET models for three crops on all satellite image acquisition dates.

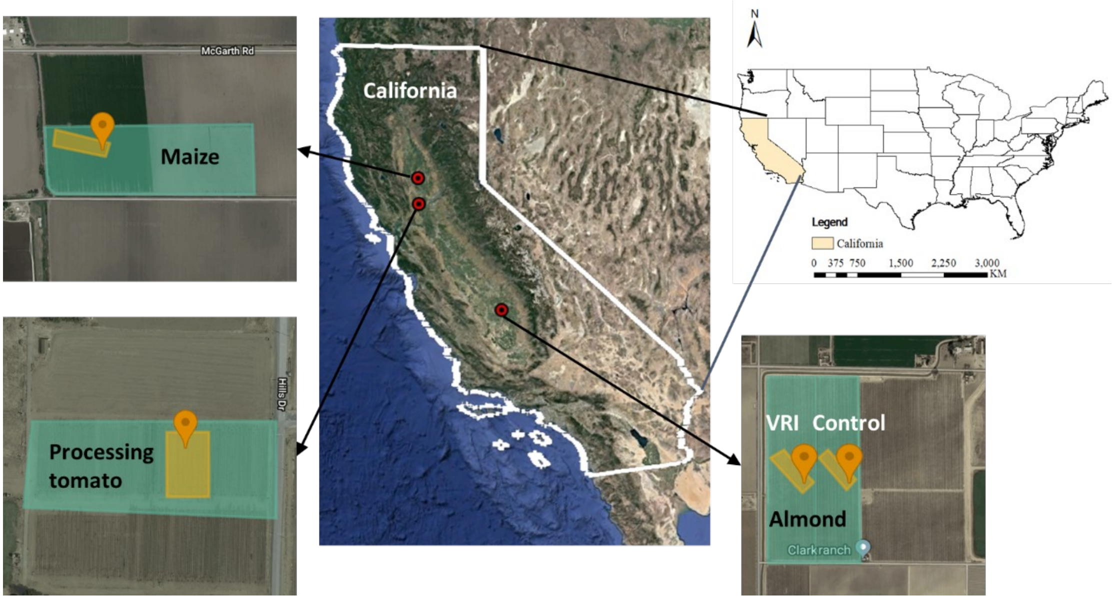

Fig. 1 Locations of field sites in the Central Valley of California. Orange point marks indicate locations of Tule surface renewal stations and the yellow rectangles represent the ET measurement areas of the Tule sensors, note that the almond orchard had an experiment of VRI (variable rate irrigation) versus control. Note that the size of ET measurement area are 207m*65m for maize field, 105m*67m for processing tomato and 167m*88m*2 for almond field.

(a) (b) (c)

Fig. 2. Comparison of the estimated daily ET$_a$ from the pySEBAL, METRIC, and SEBS models and measured daily *ET* from surface renewal method in almond (a, b, c), processing tomato (d, e, f) and maize (g, h, i).

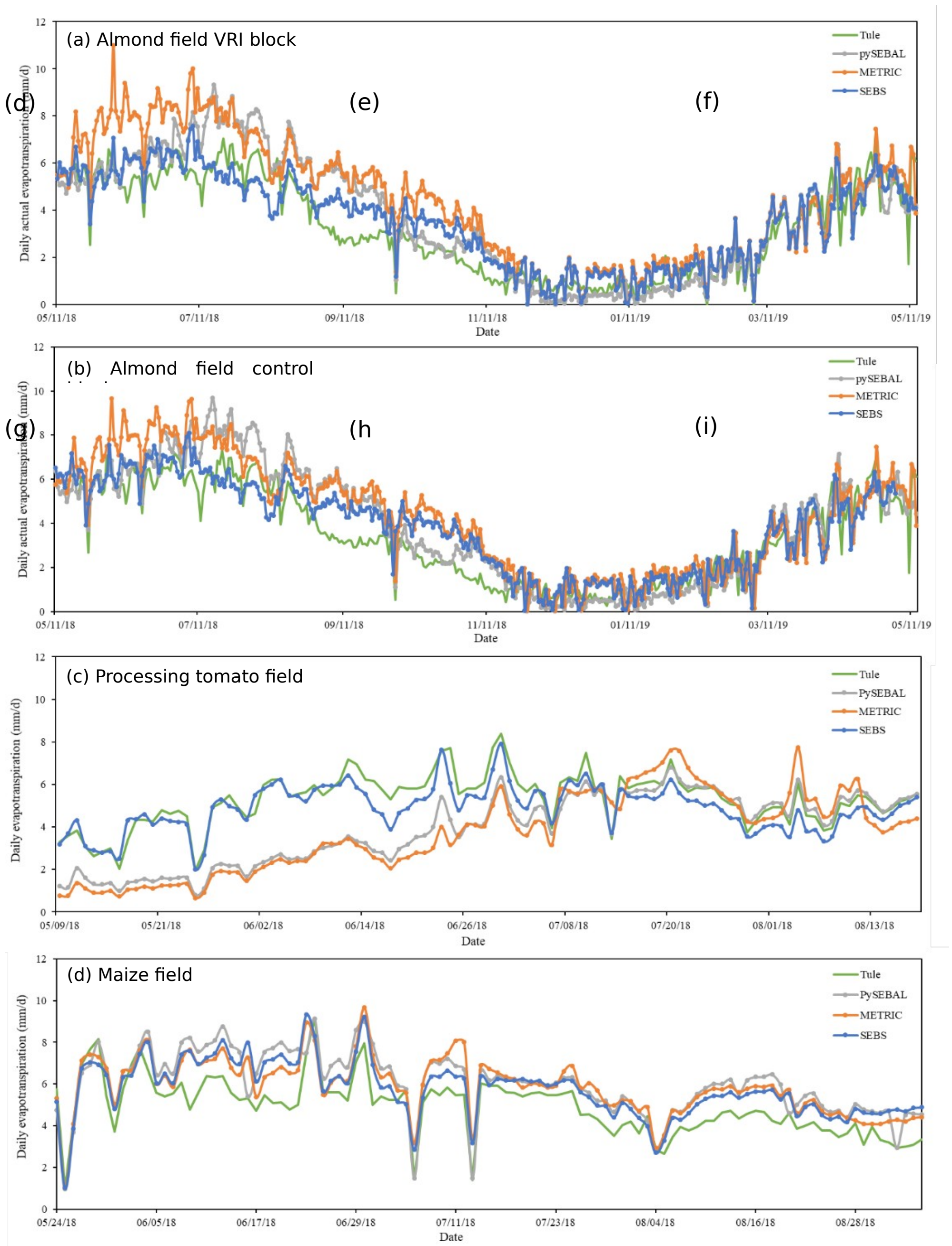

Fig. 3. Time series of daily ET$_a$ based on three RS-based models (pySEBAL, METRIC, and SEBS) and surface renewal (Tule) for the (a-b) almond, (c)

processing tomatoes and (d) maize field sites. Daily RS-based ET_a values were linearly interpolated between two satellite overpass dates.

(a) Almond

Fig. 4. Density plots of pairwise comparison of estimated daily ET_a using three RS-based ET models for (a) almond, (b) processing tomatoes and (c) maize. Note that different colors in the density plots refer to the frequency of data points at each location, with red for low frequency and blue for high frequency.

(b) Processing tomato

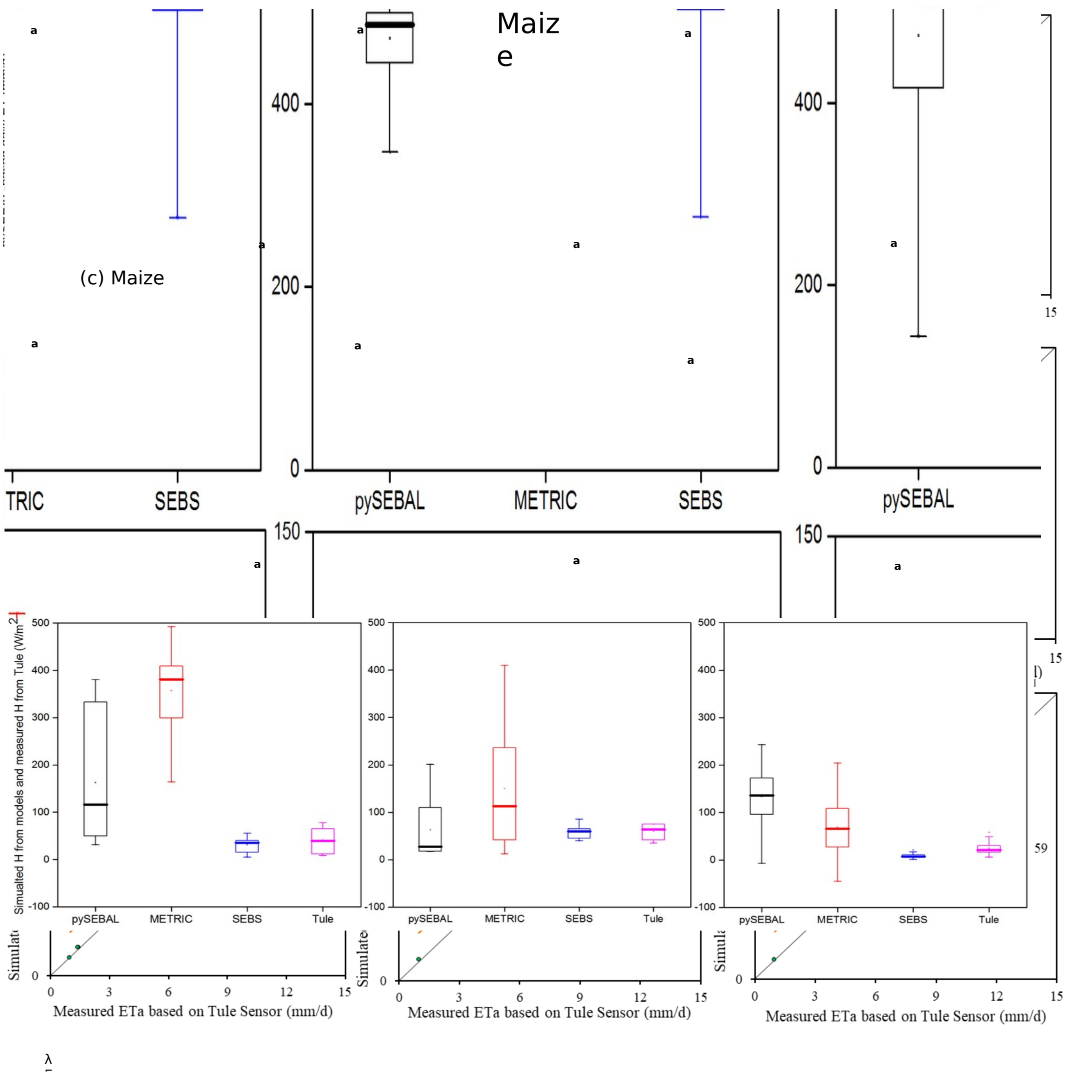

Fig. 5. Boxplots of inter-comparison of simulated and measured

instantaneous energy balance fluxes (R_n, G, H and λE) using three RS-based ET models for three crops on all satellite image acquisition dates.